VSP

Advanced Robotics 23 (2009) 2113–2138

ADVANCED ROBOTICS
www.brill.nl/ar

Full paper

Attitude Stabilization of a Biologically Inspired Robotic Housefly *via* Dynamic Multimodal Attitude Estimation

Domenico Campolo [a,*], **Giovanni Barbera** [b], **Luca Schenato** [b], **Lijuan Pi** [c], **Xinyan Deng** [c] **and Eugenio Guglielmelli** [d]

[a] School of Mechanical & Aerospace Engineering, Nanyang Technological University, 639798 Singapore

[b] Department of Information Engineering, University of Padova, 35131 Padova, Italy

[c] Department of Mechanical Engineering, University of Delaware, Newark, DE 19716, USA

[d] Biomedical Robotics Laboratory, Campus Bio-Medico University, 00128 Roma, Italy

Received 5 June 2009; accepted 3 July 2009

Abstract

In this paper, we study sensor fusion for the attitude stabilization of micro aerial vehicles, particularly mechanical flying insects. Following a geometric approach, a dynamic observer is proposed that estimates attitude based on kinematic data available from different and redundant bioinspired sensors such as halteres, ocelli, gravitometers, magnetic compass and light polarization compass. In particular, the traditional structure of complementary filters, suitable for multiple sensor fusion, is specialized to the Lie group of rigid-body rotations $SO(3)$. The filter performance based on a three-axis accelerometer and a three-axis gyroscope is experimentally tested on a 2-d.o.f. support, showing its effectiveness. Finally, attitude stabilization is proposed based on a feedback scheme with dynamic estimation of the state, i.e., the orientation and the angular velocity. Almost-global stability of the proposed controller in the case of dynamic state estimation is demonstrated *via* the separation principle, and realistic numerical simulations with noisy sensors and external disturbances are provided to validate the proposed control scheme.

Keywords

Attitude control on $SO(3)$, separation principle, geometric control, complementary filtering, biologically inspired robots

1. Introduction

The development of unmanned aerial vehicles has been a very active area of research for both civil and military applications. Many remarkable achievements have

* To whom correspondence should be addressed. E-mail: d.campolo@ntu.edu.sg

 DOI:10.1163/016918609X12529306840253

been obtained with large fixed and rotary aircraft; however, their use in many tasks is limited by their maneuverability and size. In order to overcome these limitations, the extraordinary flight capabilities of insects have inspired the design of small micro aerial vehicles (MAVs) and, in particular, of inch-size robots with flapping wings mimicking real flying insects [1]. Their unmatched maneuverability, low fabrication cost and small size make them very attractive for cost-critical missions in environments that are impenetrable for larger size UAVs such as helicopters or airplanes. Moreover, the latest progresses in insect flight aerodynamics [2] and in micro-technology [3] are providing sufficient tools to fabricate flying insect micro-robots, as shown by the recent take-off of a flapping flight robotic insect [4]. Although many problems remain to be solved in terms of fabrication and electromechanical design, the next fundamental challenge to be undertaken is the design of control architectures and algorithms to control and navigate flapping flight robotic insects. It has been observed by biologists that insects can control the generation of forces and torques by modulating the wing kinematics trajectories [2, 5]. This observation has suggested the use of averaging theory tools and a bioinspired parameterization of the wing kinematics to decouple the wing control design from the attitude control design [6, 7]. This approach has been shown successful also in other biomimetic forms of locomotion, e.g., fish swimming [8], and greatly simplifies the design of an autonomous navigation systems, since it naturally leads to a hierarchical architectures [7].

Based on these considerations, in this paper, we focus on the design of attitude control that uses as inputs the signals coming from bioinspired sensors such as ocelli, halteres, magnetometers and gravitometers. The ability of controlling attitude in a robust and stable manner is fundamental for the design of path planning and navigation control schemes. Previous work exists in this context. For instance, in Ref. [9] the authors propose a static output feedback scheme for hovering recovery; however, this scheme is sensitive to measurement noise and external disturbances, and moreover cannot be easily extended to attitude maneuvering or control schemes based on body orientation. Rifai *et al.* [10] provide an attitude control scheme that takes into account saturation limits, but they do not consider sensors and assume to have access to exact body orientation and angular velocity. Finally, Epstein *et al.* [11] propose a dynamic output feedback schemes based on a linearized model of the insect dynamics suitable for longitudinal control or other simple flight modes, but not for more aggressive maneuvers. Here, we propose a dynamic output feedback control scheme that is globally stable and that is based on state estimation from redundant measurements, making it more robust to external disturbances and measurement noise. In particular, we show that we can decouple the orientation estimation problem from the attitude control problem. Although this separation principle is classical for linear dynamical systems, it is hard to guarantee for general nonlinear systems and, in particular, for the Lie group of rigid-body orientations $SO(3)$. Although this scheme has been specifically designed for robotic flying insects with bioinspired sensors, it is rather general and can be used also

for more traditional UAVs as long as the output signals are 'linear' in the rotation matrix, as explained later. In fact, this scheme has the advantage of being globally stable differently from more traditional control strategies based on extended Kalman filters (EKFs).

As for the outline of the paper, Section 3 briefly describes the attitude dynamics of a robotic flying insect and reviews navigation sensory systems of real insects. Section 4 presents a complementary filter for sensor fusion as well as the experimental validation of its performance. Section 5 proposes a control feedback based on the dynamic attitude estimation that is proven to be globally stable *via* the separation principle and it is tested using realistic numerical simulations. Before proceeding some mathematical background is presented.

2. Mathematical Background

This section briefly describes the notation and several geometric notions that will be used throughout the paper. For additional details, the reader is referred to texts such as Refs [12–16].

2.1. Basic Definitions

As shown in Refs [12, 13], the natural configuration space for a rigid body is the Lie group $SO(3)$, i.e., the configuration of a rigid body can always be represented by a rotation matrix R, i.e., a matrix such that $R^{-1} = R^{\mathrm{T}}$ and $\det R = +1$.

Consider now the coordinate frames $\mathbb{R}^3_{\mathrm{S}}$ and $\mathbb{R}^3_{\mathrm{B}}$:

- $\mathbb{R}^3_{\mathrm{S}} \approx \mathbb{R}^3$: the space coordinate frame, or initial configuration frame.
- $\mathbb{R}^3_{\mathrm{B}} \approx \mathbb{R}^3$: the body frame, which is attached to the body (can be thought of as defined by the sensors sensitive axis), initially coincident with the space frame.

An element R of $SO(3)$ can be thought of as a map from the body frame to the space frame, i.e., $R : \mathbb{R}^3_{\mathrm{B}} \to \mathbb{R}^3_{\mathrm{S}}$.

A trajectory of the rigid body is curve $R(t) : \mathbb{R} \to SO(3)$. The velocity vector $\dot{R}$ is tangent to the group $SO(3)$ in R but, as shown in Refs [12, 13], rather than considering $\dot{R}$, two important quantities are worth to be considered:

- $\dot{R}R^{\mathrm{T}}$: representing the rigid body angular velocity relative to the space frame.
- $R^{\mathrm{T}}\dot{R}$: representing the rigid body angular velocity relative to the body frame.

These are both elements of the Lie algebra $so(3)$, i.e., the tangent space to the group $SO(3)$ at the identity I.

Elements of the Lie algebra are represented by skew-symmetric matrices. Systems on Lie groups described in terms of body (space) coordinates are called left-invariant (right-invariant).

- *Left-invariance*. Let $R_1(t)$ be a trajectory of a rigid body relative to a space frame $\mathbb{R}^3_{\mathrm{S}_1}$. Consider a change of space frame $G : \mathbb{R}^3_{\mathrm{S}_1} \to \mathbb{R}^3_{\mathrm{S}_2}$, now $R_2(t) =$

$GR_1(t)$ represents the same trajectory but with respect to the new space frame. It is straightforward to verify that $R_2^{\mathrm{T}}\dot{R}_2 = R_1^{\mathrm{T}}\dot{R}_1$, i.e., the angular velocity relative to the body frame $R^{\mathrm{T}}\dot{R}$ does not depend on the choice of space frame.

- *Right-invariance*. Similarly, it can be shown that the angular velocity of a rigid body relative to a space frame $\dot{R}R^{\mathrm{T}}$ does not depend on the choice of coordinate frame attached to the body.

In the case of $SO(3)$, there exists [13] an isomorphism of vector spaces $\widehat{\cdot}: so(3) \to \mathbb{R}^3$, referred to as the hat operator, that allows writing $so(3) \approx \mathbb{R}^3$. For a given vector $\mathbf{a} = [a_1 \;\; a_2 \;\; a_3]^{\mathrm{T}} \in \mathbb{R}^3$, we write:

$$\widehat{\cdot}: \mathbf{a} = \begin{bmatrix} a_1 \\ a_2 \\ a_3 \end{bmatrix} \longrightarrow \begin{bmatrix} 0 & -a_3 & a_2 \\ a_3 & 0 & -a_1 \\ -a_2 & a_1 & 0 \end{bmatrix} = \widehat{\mathbf{a}}. \tag{1}$$

Denote $(\cdot)^{\vee}: \mathbb{R}^3 \to so(3)$ its inverse, referred to as the vee operator:

$$(\cdot)^{\vee}: \widehat{\mathbf{a}} = \begin{bmatrix} 0 & -a_3 & a_2 \\ a_3 & 0 & -a_1 \\ -a_2 & a_1 & 0 \end{bmatrix} \longrightarrow \begin{bmatrix} a_1 \\ a_2 \\ a_3 \end{bmatrix} = (\widehat{\mathbf{a}})^{\vee}. \tag{2}$$

The Lie algebra is equipped with an operator, the Lie brackets $[\cdot, \cdot]$, is defined by the matrix commutator:

$$[\widehat{\mathbf{a}}, \widehat{\mathbf{c}}] = \widehat{\mathbf{a}}\,\widehat{\mathbf{c}} - \widehat{\mathbf{c}}\,\widehat{\mathbf{a}} = \widehat{\mathbf{a} \times \mathbf{c}}, \tag{3}$$

where $\mathbf{a}, \mathbf{c} \in \mathbb{R}^3$, $\widehat{\mathbf{a}}, \widehat{\mathbf{c}} \in so(3)$ and $\times$ is cross-product in $\mathbb{R}^3$.

Given a finite-dimensional vector space V, let V^* be its dual space, i.e., the space whose elements (covectors) are linear functions from V to $\mathbb{R}$. If $\boldsymbol{\sigma} \in V^*$, then $\boldsymbol{\sigma}: V \to \mathbb{R}$. Denote the value of $\boldsymbol{\sigma}$ on $\mathbf{v} \in V$ by $\langle \boldsymbol{\sigma}, \mathbf{v} \rangle$, i.e., the pairing operator $\langle \cdot, \cdot \rangle: V^* \times V \to \mathbb{R}$.

If $V = \mathbb{R}^n$ then $V^* \simeq \mathbb{R}^n$. For all $\mathbf{v} \in V$ and $\boldsymbol{\sigma} \in V^* \simeq R^n$ then:

$$\begin{aligned} \langle \boldsymbol{\sigma}, \mathbf{v} \rangle &= \boldsymbol{\sigma}^{\mathrm{T}}\mathbf{a} \\ \langle \widehat{\boldsymbol{\sigma}}, \widehat{\mathbf{v}} \rangle &= \frac{1}{2}\,\mathrm{trace}(\widehat{\boldsymbol{\sigma}}^{\mathrm{T}}\widehat{\mathbf{v}}). \end{aligned} \tag{4}$$

2.2. *Metric Properties of* SO*(3)*

In what follows, the necessary background and geometric tools are reviewed in order to define a norm (a distance) on $SO(3)$. This will be used later to prove convergence of the proposed feedback.

On a general manifold M, a positive definite quadratic form $\langle\langle \boldsymbol{\xi}_1, \boldsymbol{\xi}_2 \rangle\rangle_{T_xM}$ defined on any tangent space $T_xM \ni \boldsymbol{\xi}_1, \boldsymbol{\xi}_2$ (the space tangent to M in $x \in M$) is called a Riemannian metric [12]. It is the equivalent of the scalar product in $\mathbb{R}^n$ and can be used to measure the distance between different points of a manifold; in mechanics a metric is tightly linked to the definition of kinetic energy [16]. A metric is an extra structure and does not come with the manifold. Many different metrics, i.e., many different distance measures, can be defined on the same manifold [12].

Lie groups are, by definition, manifolds and, therefore, are entitled to posses metric properties. Lie groups, in particular $SO(3)$, are structured in such a way that some metrics naturally arise (natural means that it does not depend on a particular choice of coordinates). A left-invariant metrics does not depend on the choice of the space frame, i.e., it only needs to be defined on the Lie algebra and then it can be left-translated to the tangent space at any other group element:

$$\langle\langle R\widehat{\mathbf{a}}, R\widehat{\mathbf{c}}\rangle\rangle_{T_R SO(3)} = \langle\langle \widehat{\mathbf{a}}, \widehat{\mathbf{c}}\rangle\rangle_{so(3)},$$

where $R \in SO(3)$ and $\widehat{\mathbf{a}}, \widehat{\mathbf{c}} \in so(3)$.

Still, there many choices for a metric in the Lie algebra — as many as there are positive definite matrices P:

$$\langle\langle \widehat{\mathbf{a}}, \widehat{\mathbf{c}}\rangle\rangle_{so(3)} \stackrel{\Delta}{=} \mathbf{a}^{\mathrm{T}} P \mathbf{c},$$

where $\mathbf{a}, \mathbf{c} \in \mathbb{R}^3$ correspond to $\widehat{\mathbf{a}}, \widehat{\mathbf{c}} \in so(3)$ as in (1). However, there only exists one choice (up to a coefficient [12, 13, 16, 17]) when the metrics needs to be bi-invariant (i.e., both right- and left-invariant):

$$\langle\langle \widehat{\mathbf{a}}, \widehat{\mathbf{c}}\rangle\rangle_{so(3)} \stackrel{\Delta}{=} \mathbf{a}^{\mathrm{T}} I \mathbf{c} = \mathbf{a}^{\mathrm{T}} \mathbf{c} = \langle \mathbf{a}, \mathbf{c}\rangle, \tag{5}$$

where I is the 3×3 identity matrix.

Two main results provided in Ref. [17] are:

- The existence of a natural norm (which measures the distance between R and the identity I) on $SO(3)$:

$$\|R\|_{SO(3)} = \langle\langle \widehat{\boldsymbol{\phi}}_R, \widehat{\boldsymbol{\phi}}_R\rangle\rangle_{so(3)}^{1/2} = \|\boldsymbol{\phi}_R\|_{\mathbb{R}^3}. \tag{6}$$

- A formula for computing its time derivative on the Lie algebra $so(3)$:

$$\frac{1}{2}\frac{\mathrm{d}}{\mathrm{d}t}\|R(t)\|_{SO(3)} = \langle\langle \widehat{\boldsymbol{\phi}}_R, R^{\mathrm{T}}\dot{R}\rangle\rangle_{so(3)} R^{\mathrm{T}} >_{so(3)}, \tag{7}$$

  where $\widehat{\boldsymbol{\phi}}_R \in so(3)$, also referred to as $\log R$, is defined as the angular velocity that takes the rigid body from I to $R \in SO(3)$ in one time unit; see Ref. [13] for details on the logarithmic map:

$$\widehat{\boldsymbol{\phi}}_R = \log R = \frac{\theta_R}{2\sin\theta_R}(R - R^{\mathrm{T}}), \tag{8}$$

  where, for $\mathrm{trace}(R) \neq -1$, θ_R satisfies $1 + 2\cos\theta_R = \mathrm{trace}(R)$ and $\|\phi_R\|^2 = \theta_R^2$, and the Rodrigues formula:

$$R = \exp(\widehat{\boldsymbol{\phi}}_R) = I + \alpha_R \widehat{\boldsymbol{\phi}}_R + \beta_R \widehat{\boldsymbol{\phi}}_R^2, \tag{9}$$

  where $\alpha_R = \|\boldsymbol{\phi}_R\|^{-1} \sin\|\boldsymbol{\phi}_R\|$ and $\beta_R = (1 - \cos\|\boldsymbol{\phi}_R\|)\|\boldsymbol{\phi}_R\|^{-2}$.

3. Biologically Inspired Robotic Housefly

In this section we review the most important features of a micromechanical flying insect, summarizing some of the results presented in Refs [6, 7].

3.1. Dynamics of the Micromechanical Flying Insect

Insect flight dynamics is still a very active area of research. In particular, there is great interest in understanding the unsteady state nature of flapping wings aerodynamics, which is believed to be source of the high maneuverability of insect flight as compared to fixed-winged vehicles and helicopters [18]. A detailed discussion of flying insect aerodynamics and modeling is beyond the scope of this paper, and we address the interested readers to the recent paper by Deng *et al.* and references therein [6]. Here, we simply summarize some results relevant to our discussion on attitude stabilization.

Since the mass of the wings is negligible with respect to the body mass, the dynamics of a flying insect can be modeled as the dynamics of a rigid-body subject to external forces and torques. In particular, as long as attitude is concerned, the dynamics is described by:

$$J\dot{\boldsymbol{\omega}} = \boldsymbol{\tau}_{\text{aero}} - \boldsymbol{\omega} \times J\boldsymbol{\omega}, \tag{10}$$

where J is the moment of inertia of the insect, $\boldsymbol{\tau}_{\text{aero}}$ is the total external torque with respect to the insect center of mass in the body frame due to the aerodynamic forces generated by the flapping wings and $\boldsymbol{\omega}$ is the angular velocity with respect to the body.

The dynamics of (10), affine with respect to the forcing input $\boldsymbol{\tau}_{\text{aero}}$, can be averaged out as in Ref. [7]. The time-varying components of the torque can be neglected while the mean value of the torque $\boldsymbol{\tau}_{\text{FB}}$ will be used as the feedback (FB) term for attitude stabilization. As this term depends upon the current orientation R and the current angular velocity $\boldsymbol{\omega}$, the averaged attitude dynamics of a mechanical flying insect are described by the system:

$$\begin{cases} \dot{R} = R\widehat{\boldsymbol{\omega}} \\ \dot{\boldsymbol{\omega}} = J^{-1}(J\boldsymbol{\omega} \times \boldsymbol{\omega} + \boldsymbol{\tau}_{\text{FB}}(R, \boldsymbol{\omega})), \end{cases} \tag{11}$$

where the $\widehat{\cdot}$ hat operator transforms the $\boldsymbol{\omega}$ vector into a skew-symmetric matrix $\widehat{\boldsymbol{\omega}}$ and $(R, \boldsymbol{\omega})$ is an element of $SO(3) \times so(3)$, i.e., the product space of the Lie group $SO(3)$ of rigid body rotations and its algebra $so(3)$.

3.2. Sensory System of Flying Insects

The highly specialized sensory system of flying insects is at the base of their extraordinary flying performance. In fact, flying insects can rely on an heterogeneous set of redundant sensors for controlling flight maneuvers and navigate the environment. Redundancy is the key to robustness. Some of these sensors represent a rich source of inspiration for the design of mechanical flying insects [6, 19] and they motivate the control strategy proposed in this work.

3.2.1. Halteres

The halteres are club-shaped small appendages behind each wing that oscillate in anti-phase with respect of the wing, as shown in Fig. 1. The plane of oscillation is slightly tilted toward the tail of the insect to be able to measure Coriolis forces

Figure 1. Photo of a fly haltere. Courtesy of Ref. [23].

along all three body axes [20]. The halteres function as tiny gyroscopes and through appropriate signal processing [21] they can reconstruct the body angular velocity vector:

$$\mathbf{y}_{\mathrm{hl}} = \boldsymbol{\omega}. \tag{12}$$

Recently, preliminary prototypes of micro-electromechanical halteres have been fabricated and have shown promising results [22].

3.2.2. Mechanoreceptors

Many parts of the insect body such as wings, antennae, neck and legs are innervated by campaniform sensilla. These cells can measure and encode pressure forces when they are stretched or strained [24]. For example, sensilla at the base of wing hinges can measure aerodynamic forces, which are used to fine-tune the wing motion. Similarly, the sensilla on the legs might be used to measure the gravity sensor, thus acting as a gravitometer. Therefore, in static conditions, insect can measure the gravity vector with respect to the body frame, i.e.:

$$\mathbf{y}_{\mathrm{g}} = R^{\mathrm{T}}\mathbf{g}_0, \tag{13}$$

where $\mathbf{g}_0$ are the (known) gravity vector components, measured with respect to the fixed frame. In non-static conditions, also non-inertial accelerations add up to the output of mechanoreceptors, as a form of disturbance. Combining information

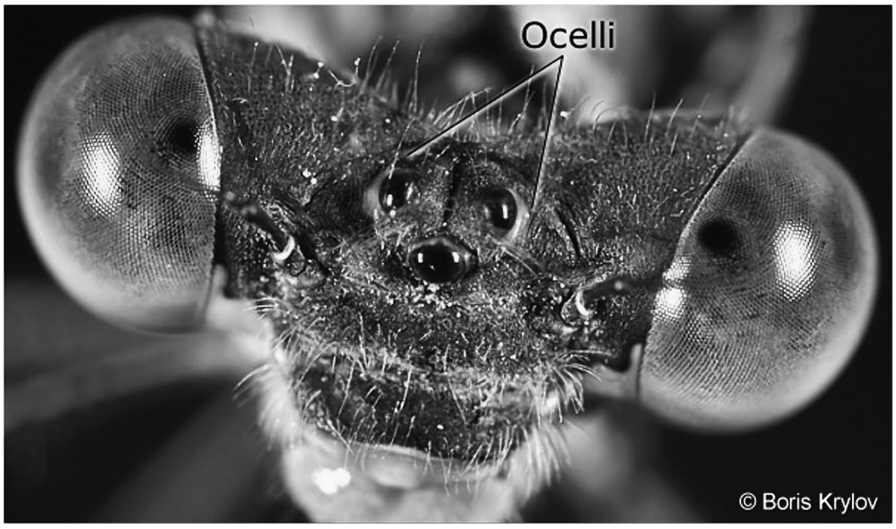

Figure 2. Photo of a fly's head showing compound eyes and the ocelli with its three photoreceptors. Courtesy of Ref. [26].

from mechanoreceptors and halteres (sensor fusion) can greatly alleviate the effects of such disturbances.

3.2.3. Ocelli

The ocelli are three additional light-sensitive organs located at the vertices of an imaginary triangle on the middle of head of the insect as shown in Fig. 2, and provide signals that are used for stabilization with respect to the rapid perturbations in roll and pitch [19]. In fact, these sensors collect and measure light intensity from a portion of the sky, and they estimate the position of the sun with respect to the insect body by comparing the signals from the left and right ocelli to estimate the roll angle, and by comparing the signal from the forward-looking ocellus with the mean of the signals from the left and the right ocelli to estimate the pitch angle [25].

3.2.4. Compound Eyes

The compound eyes of the insects are an advanced vision system that processes different types of signals needed for the optomotor systems. In fact they can process the visual stimuli to estimates angular velocities thanks to large-field neurons that are tuned to respond to the specific patterns of optic flow that are generated by yaw, roll and pitch [27], as well as body orientation and position by higher-level visual processing like object fixation and landmark detection for navigation and path planning [11]. However, such signals require quite a specialized signal processing system that might not be necessary for attitude stabilization, which is the objective of this work. However, the dorsally directed (upward-looking) regions of the compound eyes of many insects are equipped with specialized photoreceptors that are sensitive to the polarized light patterns that are created by the sun in the sky. More

precisely, insects can measure their orientation relative to the direction of the light polarization: $\mathbf{p}_0 \in \mathbb{R}^3$, as:

$$\mathbf{y}_\mathrm{p} = R^\mathrm{T}\mathbf{p}_0. \tag{14}$$

Differently from the ocelli, the light polarization direction is not affected by light intensity. Bioinspired polarized light compasses are easier to fabricate than the full insect visual system, and have been successfully fabricated and used for robot navigation [28], and are relevant to the flight control design proposed in this work.

3.2.5. Magnetic Compass

Recent studies indicate that some insects can also detect the Earth's magnetic and this is used to maintain a desired heading direction [29]. Similarly to the light polarization sensor, we can argue that insects can measure the components of the magnetic field with respect to the body as follows:

$$\mathbf{y}_\mathrm{m} = R^\mathrm{T}\mathbf{b}_0, \tag{15}$$

where $\mathbf{b}_0 \in \mathbb{R}^3$ is the direction of the magnetic field relative to the fixed frame. A possible electromechanical implementation of a magnetic compass suitable for small-size vehicles is given in Ref. [30].

4. Sensor Fusion *via* Complementary Filters

The sensory system of real insects is clearly redundant, e.g., kinematic quantities such as the angular velocity are derived from more than one sensor. Information from different sensors is then 'fused' together. Complementary filters traditionally arise in applications where redundant measurements of the same signal are available [31] and the problem is combining all available information in order to minimize the instrumentation error.

For the sake of simplicity, consider only two sensors, s_1 and s_2, providing readings of the same quantity, e.g., the angular velocity ω, with different noise characteristics, i.e., $s_1 = \omega + n_1$ and $s_2 = \omega + n_2$, where $\|n_1\| < \|n_2\|$ at high frequency while $\|n_2\| < \|n_1\|$ at low frequency. Then a low-pass filter $L(s)$ and its complementary high-pass filter $H(s) = 1 - L(s)$ can be used to fuse information:

$$s_\mathrm{fusion} = s_1 H(s) + s_2 L(s) = \omega + n_2 L(s) + n_1(1 - L(s)), \tag{16}$$

from two or more sensors (e.g., halteres, ocelli and compound eyes). The cut-off frequency of the filter $L(s)$ can be chosen so that the spectral content of $n_2 L(s) + n_1(1 - L(s))$ will be less than the spectral content of n_1 or n_2 [31].

The kinematic variable ω is dynamically unaffected by the filter. The estimated variable (i.e., the output of the filter) is related to the input variable *via* a purely algebraic relation in the time domain and no dynamics are involved in the noiseless case. Such filters can be safely used in feedback loops to fuse readings of the same kinematic variable from different sensors since no extra dynamics is added to the overall system and stability (which involves noiseless conditions) is not affected.

Complementary filters can be generalized to fuse information derived from sensors when the sensed variables are related by differential equations, e.g., position and speed. In these cases, the filter introduces some dynamics between the estimated output and the sensed inputs.

The differential equations relating the sensed variables may be nonlinear, which is typically the case when attitude is concerned. Theory of complementary and Kalman filters have been traditionally used to design attitude filters. Although the Kalman filters can be extended (EKF) to nonlinear cases, they fail in capturing the nonlinear structure of the configuration space of problems involving, for example, rotations of a rigid body and, most importantly, they can run into instabilities. On the other hand, nonlinear filters [32], in particular complementary filters, can better capture such a nonlinear structure.

4.1. Dynamic Attitude Estimation

As an example of use of complementary filters when different kinematic variables are involved, consider the linear case of a rotational mechanical system with 1 d.o.f. (θ). As shown in Ref. [31], complementary filters such as the one represented in Fig. 3 are traditionally used to fuse information available from both angular position sensors and tachometers, respectively, θ_{sens} and ω_{tacho}. Let θ^* be the estimate of θ. The filter gain k in Fig. 3 determines the transition frequency of the filter after which the data from the tachometer (ω_{tacho}) are weighted more, whereas before the transition frequency data from the position sensors (θ_{sens}) are predominant on the dynamic equation (the integrator $1/s$). The optimal value for k is in fact determined from the spectral characteristics of measurement noise [31].

Differently from the previous example, $SO(3)$ is a nonlinear space and that is where the advantages of a geometric approach can be fully appreciated. A part from nonlinear dynamics, the very definition of estimation errors requires caution. In the linear case, $e = \theta - \theta^*$ is a typical choice while quantities such as $R - R^*$ with R, $R^* \in SO(3)$ are no longer guaranteed to belong to $SO(3)$. Following [17], the estimation error will be defined as $E = R^{\mathrm{T}} R^*$.

A complementary filter on $SO(3)$ was presented in Ref. [33] for dynamic attitude estimation. The main definition, theorem and related lemmas are reported in

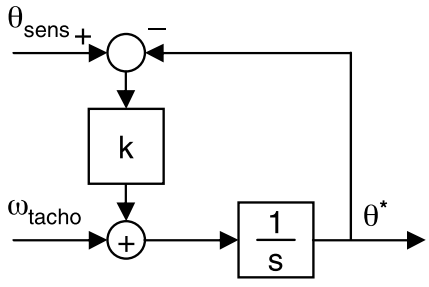

Figure 3. Linear complementary filter for a rotational mechanical system with 1 d.o.f.

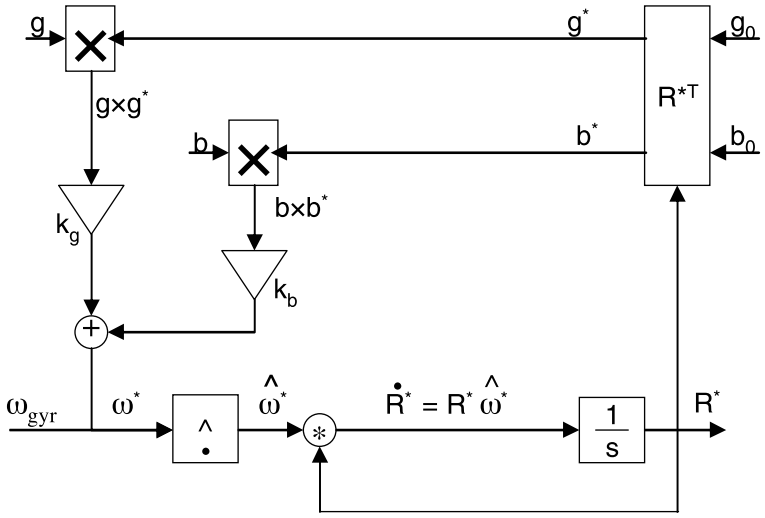

Figure 4. Complementary filter for dynamic attitude estimation.

Appendix A for convenience; the interested reader can refer to Ref. [33] for the proof.

A block diagram of the filter, for the specific case of interest, is shown in Fig. 4. Raw data from gyroscopes ($\boldsymbol{\omega}_{\text{gyr}}$), from accelerometers ($\mathbf{g}$) and from magnetometers ($\mathbf{b}$) (i.e., a total of nine channels) are fused together to provide an estimate of the orientation (R^*). The filter also uses two initial readings $\mathbf{g}_0$ and $\mathbf{b}_0$, respectively, from accelerometers and magnetometers. The orientation matrix R^* can be initially set to any appropriate value (e.g., the 3×3 identity matrix) in the integration block.

As a final note, in linear cases such as in Fig. 3 all the variables belong to the same space $\mathbb{R}^n$. In the nonlinear filter in Fig. 4, variables in different nodes of the block diagram belong to very different spaces, some linear ($so(3)$) and some nonlinear ($SO(3)$). The adopted geometric approach leads us to recognize how sensor fusion naturally occurs on the linear space of angular velocities, i.e., the Lie algebra $so(3)$.

4.2. Numerical Implementation

The filter in Fig. 4, in principle, can be directly implemented in simulation environments such as Matlab/Simulink from MathWorks. Any digital implementation of the filter would (i) transform the filter in a discrete-time one with time sequence t_n and (ii) necessarily introduce numerical errors. The main risk is that, as numerical errors accumulate, quantities such as $R_n^* = R^*(t_n)$ are likely to drift away from $SO(3)$, i.e., $\det R_n^*$ very different from 1 and/or $R_n^{*\mathrm{T}} R_n^*$ very different from the identity matrix I. This can be avoided by considering that data from analog sensors are typically acquired *via* digital-to-analog converters with a fixed sampling time; let this sampling time be ΔT. In the time interval $t_n \leqslant t < t_{n+1} = t_n + \Delta T$, data

from sensors can be assumed constantly equal to the last sampled value. This allows computing R^*_{n+1} *via* the Rodrigues formula [13] as:

$$\begin{aligned}
\boldsymbol{\omega}^*_n &= \boldsymbol{\omega}_n + k_{\mathrm{g}}(\mathbf{g}_n \times (R^{*\mathrm{T}}_n \mathbf{g}_0)) + k_{\mathrm{b}}(\mathbf{b}_n \times (R^{*\mathrm{T}}_n \mathbf{b}_0)) \\
\alpha_n &= \sin \|\Delta T \widehat{\boldsymbol{\omega}}^*_n\| / \|\Delta T \widehat{\boldsymbol{\omega}}^*_n\| \\
\beta_n &= (1 - \cos \|\Delta T \widehat{\boldsymbol{\omega}}^*_n\|) / \|\Delta T \widehat{\boldsymbol{\omega}}^*_n\|^2 \\
R^*_{n+1} &= R^*_n (I + \alpha_n \Delta T \widehat{\boldsymbol{\omega}}^*_n + \beta_n \Delta T^2 \widehat{\boldsymbol{\omega}}^{*2}_n),
\end{aligned} \tag{17}$$

which is guaranteed not to drift away from $SO(3)$.

4.3. Experimental Tests of Attitude Estimation

In this section we present some experimental results relative to attitude estimation based on the complimentary filter given by (17).

4.3.1. Experimental Setup

A circuit board equipped with a pair of IDG-300 dual-axis gyroscopes (InvenSense) and one three-axis ADXL330 accelerometer (Analog Devices) was mounted on a holder, and set free to rotate about the roll (x) and pitch (y) axis (Fig. 5). The holder included two MAE-3 US-Digital angular sensors to measure the exact angular displacement. The accelerometers are used to measure the static gravity acceleration, while the gyroscopes provide the angular rate with respect to the three axes in the body reference frame.

4.3.2. Results

According to the reference frame presented in Fig. 5 and adopting the yaw–pitch–roll Euler angles (ZYX), the rotation matrix $R \in SO(3)$ can be considered as a map from the body-fixed frame to the space frame given by the sequential rotation about the Z_{b}, Y_{b} and X_{b} axis:

$$R = \begin{bmatrix} r_{11} & r_{12} & r_{13} \\ r_{21} & r_{22} & r_{23} \\ r_{31} & r_{32} & r_{33} \end{bmatrix} = R_x(-\phi) R_y(-\theta) R_z(-\psi), \tag{18}$$

ϕ, θ and ψ being the roll, pitch and yaw angles, respectively. Since this map is surjective, with only the exception of the singularity in $\theta = \pi/2$ for the pitch angle, one can directly evaluate ϕ, θ and ψ, i.e., invert (18) and, thus, immediately compare the true angular position measured by the position sensors mounted on the holder with the estimated angles from the complimentary filter. Inverting (18) yields:

$$\begin{aligned}
\theta &= -\arcsin(r_{31}) \\
\phi &= \operatorname{atan2}\left(\frac{r_{32}}{\cos(\theta)}, \frac{r_{33}}{\cos(\theta)}\right) \\
\psi &= \operatorname{atan2}\left(\frac{r_{21}}{\cos(\theta)}, \frac{r_{11}}{\cos(\theta)}\right).
\end{aligned} \tag{19}$$

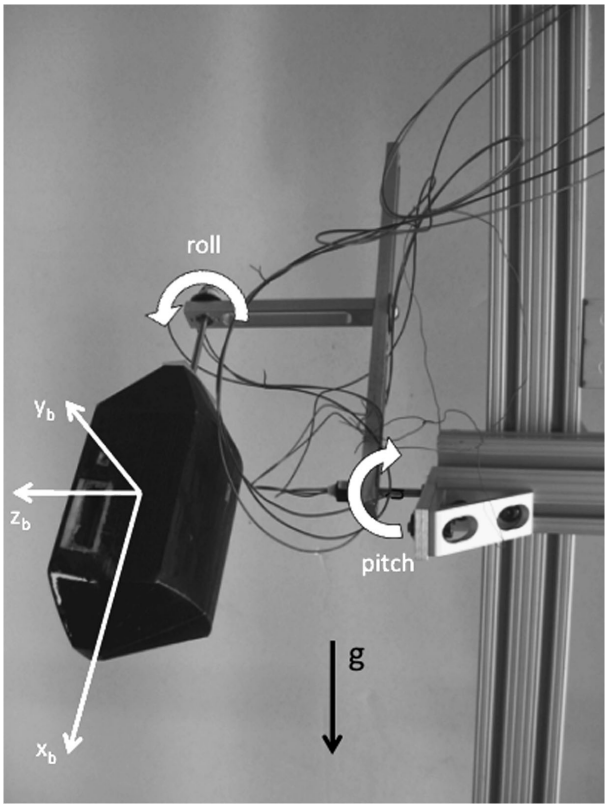

Figure 5. Support used to perform the combined roll/pitch motion. The body-fixed coordinate system is also shown.

The matrix $R^{\mathrm{T}}(t)R^{*}(t)$ is guaranteed to converge to the identity matrix I for any initial condition, i.e., the estimated orientation $R^{*}(t)$ converges to the true orientation $R(t)$, the initial condition of the complementary filter. In the experiments the initial orientation $R^{*}(t_0)$ was set to be different from the true $R(t_0)$ in order to evaluate the speed of convergence. The results of attitude estimation from the complementary filter are shown in Fig. 6, and the associated sensor readouts are shown in Figs 7 and 8. The plots show rapid convergence of the estimated angles to the true angles in the first 0.5 s of the experiments when the body frame is kept fixed and then they remain very close to the true angles during the body motion. The effectiveness of sensor fusion is best appreciated by removing either the gyros or the accelerometers from the filter. In the first case, the removal of the gyros results in an evident low-pass behavior of the estimated angles which exhibit a time lag as compared to the true angles. Differently, if only gyros are used, the estimated angles have a rapid response to body motion, but they show a drift that over time leads to large offsets as compared to the true angles. The complementary filter, as explained above, fuses the benefits from both sensor modalities, giving rise to a filter with a very high bandwidth.

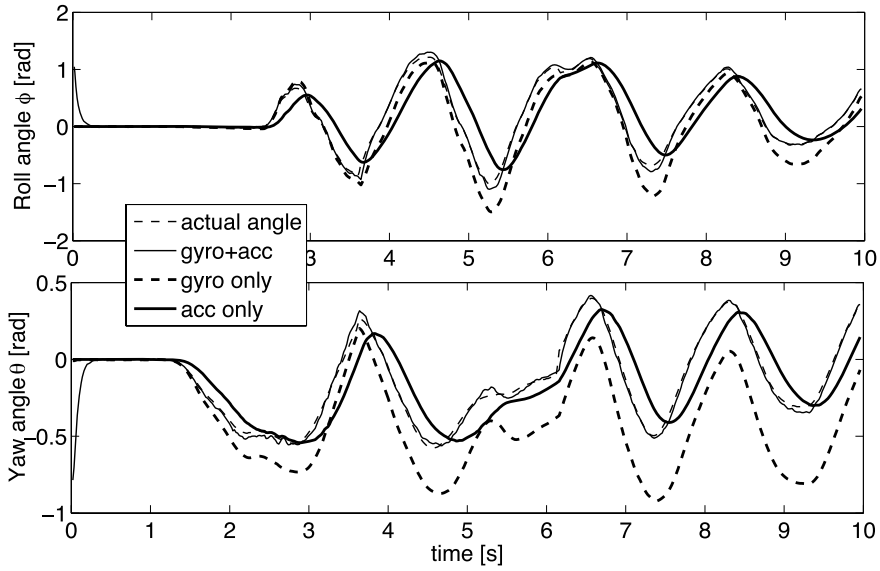

Figure 6. Comparison between the actual roll angle (top) and pitch angle (bottom), and three different estimations evaluated using only the accelerometers data, only the gyroscope data or both.

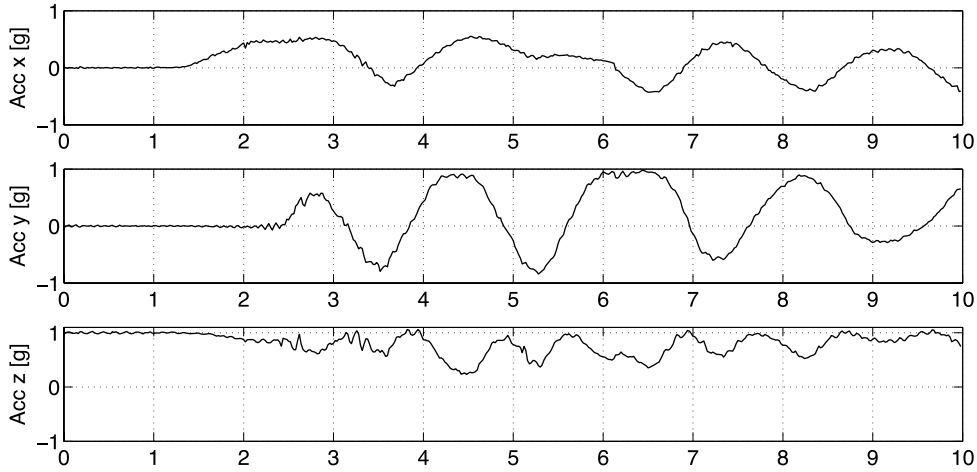

Figure 7. Accelerometer readouts. Readings are normalized with respect to gravity acceleration g.

5. Attitude Stabilization *via* the Separation Principle

In this section, results of traditional attitude control are first reviewed and then applied to derive a control law based on state feedback. Since in the application of interest the state of the system is not known and only an estimation of the current state can be used as feedback, it is natural to wonder whether dynamic output feedback control preserves the stability properties of the state feedback control, i.e., whether the separation principle holds. Maithripala *et al.* [34, 35] proved that the

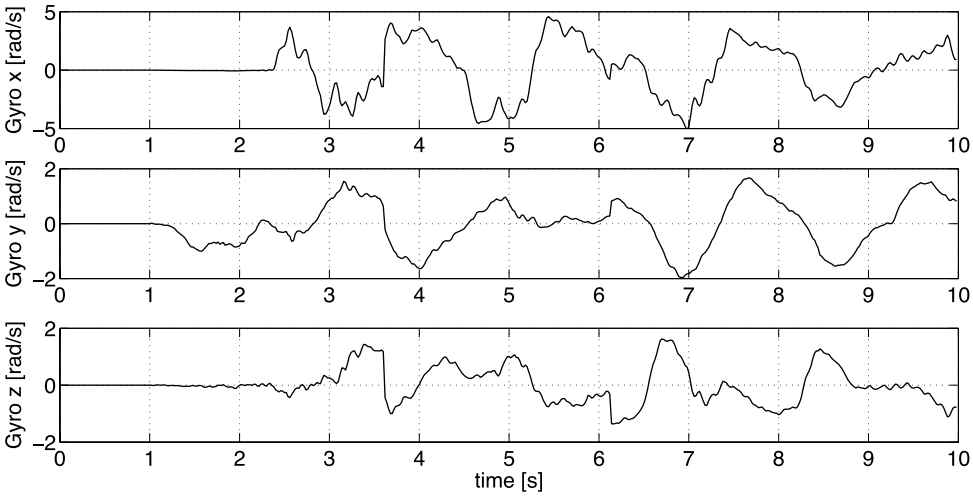

Figure 8. Gyroscopes readouts.

separation principle also holds in the general case of compact Lie groups and, therefore, also for $SO(3)$. For the reader's convenience this general result is restated in terms of $SO(3)$ in Appendix B. In this section, results from Refs [34, 35] are specialized to $SO(3)$, the Lie groups of rigid-body rotations, and traditional state feedback control is combined with the dynamic attitude observer presented in Ref. [33].

5.1. Attitude Control via State Feedback

Traditionally, control of (11) is performed *via* passivity-based arguments. Maithripala *et al.* [34] show that the system (11) can be stabilized by a state feedback torque $\boldsymbol{\tau}_{\mathrm{FB}}(R, \boldsymbol{\omega})$ that consists of a conservative part, derived from a potential (also referred to as 'error') Morse function $U : SO(3) \to \mathbb{R}$, and a dissipative (Rayleigh-type) part (a function whose critical points are non-degenerate [16]):

$$\boldsymbol{\tau}_{\mathrm{FB}}(R, \boldsymbol{\omega}) = -J(R^{\mathrm{T}} \operatorname{grad} U + k_{\boldsymbol{\omega}} \widehat{\boldsymbol{\omega}})^{\vee}, \tag{20}$$

where $\operatorname{grad} U$ is the gradient of the function $U(R)$. Differently from the differential $\mathrm{d}U$, the gradient $\operatorname{grad} U$ depends on the geometry of the space itself. The gradient is in fact defined by the following identities:

$$\begin{aligned} \dot{U}(R) &= \langle \mathrm{d}U, R\widehat{\boldsymbol{\omega}} \rangle \\ &= \langle R^{\mathrm{T}} \mathrm{d}U, \widehat{\boldsymbol{\omega}} \rangle \\ &= \langle \langle R^{\mathrm{T}} \operatorname{grad} U, \widehat{\boldsymbol{\omega}} \rangle \rangle_{so(3)}, \end{aligned} \tag{21}$$

where, for a vector space V and its dual V^*, $\langle \cdot, \cdot \rangle : V^* \times V \to \mathbb{R}$ is the pairing operator and $\langle\langle \cdot, \cdot \rangle\rangle_V : V \times V \to \mathbb{R}$ is the inner product defined *via* a proper isomorphism $J : V \to V^*$ as $\langle\langle \mathbf{a}, \mathbf{b} \rangle\rangle_V = \langle J\mathbf{a}, \mathbf{b} \rangle_V$, see Refs [33–35]. In mechanics, a natural iso-

morphism J is provided by the inertia tensor (constant in body coordinates) and so the gradient is determined by:

$$R^{\mathrm{T}} \operatorname{grad} U = J^{-1} R^{\mathrm{T}} \mathrm{d}U. \tag{22}$$

Therefore, the problem of stabilizing (11) is reduced to defining a potential function $U(R)$ on $SO(3)$ with a non-degenerate critical point in the desired configuration $\bar{R} \in SO(3)$. To this end, a commonly used potential function, first introduced by Koditschek in Ref. [36], on $SO(3)$ is:

$$U(R) \triangleq \frac{1}{2} \operatorname{trace}(K(I - \bar{R}^{\mathrm{T}} R)), \tag{23}$$

where K is a symmetric 3×3 matrix with eigenvalues $\{k_1, k_2, k_3\}$. Once the potential function $U(R)$ is defined, the gradient (and, therefore, the feedback torque) can be computed as in Ref. [37] *via* the time derivative of the error function:

$$\begin{aligned} \dot{U}(R) &= \frac{1}{2} \operatorname{trace}(K(-\bar{R}^{\mathrm{T}} \dot{R})) \\ &= \frac{1}{2} \operatorname{trace}(-K \bar{R}^{\mathrm{T}} R \widehat{\boldsymbol{\omega}}) \\ &= \frac{1}{2} \operatorname{trace}(\operatorname{skew}(K \bar{R}^{\mathrm{T}} R)^{\mathrm{T}} \widehat{\boldsymbol{\omega}}) \\ &= \langle \operatorname{skew}(K \bar{R}^{\mathrm{T}} R), \widehat{\boldsymbol{\omega}} \rangle, \end{aligned} \tag{24}$$

where $\operatorname{skew}(A) = \frac{1}{2}(A - A^{\mathrm{T}})$. This allows computing $R^{\mathrm{T}} \operatorname{grad} U$ from (22):

$$R^{\mathrm{T}} \operatorname{grad} U = J^{-1} \operatorname{skew}(K \bar{R}^{\mathrm{T}} R). \tag{25}$$

Convergence properties of systems like (11) when the state feedback (20) is used can be found in Refs [34, 35], here briefly restated for the case of interest. The proof is based on La Salle's principle [15] and involves a function $V = U(R) + \frac{1}{2} \langle \langle \widehat{\boldsymbol{\omega}}, \widehat{\boldsymbol{\omega}} \rangle \rangle_{so(3)}$ as well as a set $S \subset SO(3) \times so(3)$ defined as $S = \{(R, \boldsymbol{\omega}) \mid \dot{V} = 0\}$.

The sign of $\dot{V}$ is studied as follows:

$$\begin{aligned} \dot{V} &= \dot{U}(R) + \frac{1}{2} \dot{\boldsymbol{\omega}}^{\mathrm{T}} J \boldsymbol{\omega} + \frac{1}{2} \boldsymbol{\omega}^{\mathrm{T}} J \dot{\boldsymbol{\omega}} \\ &= \dot{U}(R) + \boldsymbol{\omega}^{\mathrm{T}} J \dot{\boldsymbol{\omega}} \\ &= \dot{U}(R) + \boldsymbol{\omega}^{\mathrm{T}} (J \boldsymbol{\omega} \times \boldsymbol{\omega} + \boldsymbol{\tau}_{\mathrm{FB}}) \\ &= \dot{U}(R) + \boldsymbol{\omega}^{\mathrm{T}} \boldsymbol{\tau}_{\mathrm{FB}} \\ &= \dot{U}(R) + \langle \langle J^{-1} \widehat{\boldsymbol{\tau}}_{\mathrm{FB}}, \widehat{\boldsymbol{\omega}} \rangle \rangle_{so(3)}, \end{aligned} \tag{26}$$

since $\boldsymbol{\omega}^{\mathrm{T}} (J \boldsymbol{\omega} \times \boldsymbol{\omega}) = 0$ for all $\boldsymbol{\omega} \in \mathbb{R}^3$.

Considering (22) and (20), then:

$$\begin{aligned} \dot{V} &= \langle \langle R^{\mathrm{T}} \operatorname{grad} U, \widehat{\boldsymbol{\omega}} \rangle \rangle_{so(3)} + \langle \langle J^{-1} \widehat{\boldsymbol{\tau}}_{\mathrm{FB}}, \widehat{\boldsymbol{\omega}} \rangle \rangle_{so(3)} \\ &= -k_{\boldsymbol{\omega}} \|\boldsymbol{\omega}\|^2, \end{aligned} \tag{27}$$

which implies $S = \{(R, \boldsymbol{\omega}) \mid \boldsymbol{\omega} = 0\}$ and:

$$\langle\langle R^{\mathrm{T}} \operatorname{grad} U, \widehat{\boldsymbol{\omega}}\rangle\rangle_{so(3)} + \langle\langle J^{-1}\boldsymbol{\tau}_{\mathrm{FB}}, \widehat{\boldsymbol{\omega}}\rangle\rangle_{so(3)} \leqslant 0, \tag{28}$$

where the inequality is strict for all $(R, \boldsymbol{\omega}) \notin S$, implying asymptotic convergence. This satisfies the Assumption 1 of Lemma 3 in Appendix B.

In order to perform attitude stabilization of the system (11) *via* state feedback (20), the current attitude R and angular velocity $\boldsymbol{\omega}$ need to be available.

Angular velocity can be directly measured from gyroscopes (e.g., fusing signals from halteres, ocelli and compound eyes), while attitude can be estimated from mechanoreceptors and magnetic compass sensors, as shown next.

5.2. Dynamic Attitude Estimation Feedback

In this section, previous results on attitude control *via* state feedback and the dynamic attitude observer are coupled *via* the separation principle, restated in Appendix B.

The full dynamic equations for the proposed attitude stabilization system are:

$$\begin{cases} \dot{R} = R\widehat{\boldsymbol{\omega}} \\ \dot{\boldsymbol{\omega}} = J^{-1}(\boldsymbol{\tau}_{\mathrm{FB}}(R^*, \boldsymbol{\omega}^*) - \boldsymbol{\omega} \times J\boldsymbol{\omega}) \end{cases} \text{attitude controller} \\ \hline \begin{cases} \dot{R}^* = R^*\widehat{\boldsymbol{\omega}}^* \\ \boldsymbol{\omega}^* = \boldsymbol{\omega}_{\mathrm{gyr}} + k_{\mathrm{b}}(\mathbf{b} \times \mathbf{b}^*) + k_{\mathrm{g}}(\mathbf{g} \times \mathbf{g}^*) \end{cases} \text{dynamic observer} \tag{29}$$

The first two equations represent the system dynamics (11) with a feedback $\boldsymbol{\tau}_{\mathrm{FB}}$ similar to (20) except that it is based on the estimates (R^* and $\boldsymbol{\omega}^*$) of the current orientation and angular velocity, instead of the actual values (R and $\boldsymbol{\omega}$). The last two equations represent the dynamics of the observer (A.5) in Appendix A where, without loss of generality, only the minimum number of independent fields (**b** and **g**) is used.

Apart from proving almost-global asymptotic stability of the proposed observer, Theorem 1 in Ref. [33] (reported in Appendix A) also provides an upper bound of the attitude estimation error E, defined as:

$$E = R^{\mathrm{T}}R^*, \tag{30}$$

based on the natural Lyapunov function [17] of the estimation error:

$$W(E) = \frac{1}{2}\|E\|^2_{SO(3)} = \frac{1}{2}\|\boldsymbol{\phi}_E\|^2, \tag{31}$$

where $\boldsymbol{\phi}_E$ is defined *via* the logarithmic map as $\widehat{\boldsymbol{\phi}}_E = \log E$.

One of the outcomes of Theorem 1 in Ref. [33] is the existence of real number $\eta > 0$ such that, if the initial estimation error $E(0)$ is such that trace $E \neq -1$ (i.e., $\|\boldsymbol{\phi}_E\| < \pi$, which is almost globally verified, see Remark 1 below), then a bound for the Lyapunov function is

$$0 < W(E) < W(E(0))\mathrm{e}^{-\eta t},$$

for all $t > 0$. This translates, *via* the (31), into an upper bound for the attitude tracking error:

$$\|\phi_E\| < c\|\phi_E(0)\|\mathrm{e}^{-\lambda t}, \tag{32}$$

where $c = W(E(0))/\|\phi_E(0)\|$ and $\lambda = \eta/2$. This satisfies Assumption 2 of Lemma 3 in Appendix B.

In order to apply the separation principle, rewrite (29) as:

$$\begin{cases} \dot{R} = R\widehat{\boldsymbol{\omega}} \\ \dot{\boldsymbol{\omega}} = J^{-1}(\boldsymbol{\tau}_{\mathrm{FB}}(R, \boldsymbol{\omega}) - \boldsymbol{\omega} \times J\boldsymbol{\omega}) + \boldsymbol{\psi}(R, \boldsymbol{\omega}, \mathbf{q}) \\ \dot{R}^* = R^*\widehat{\boldsymbol{\omega}}^* \\ \boldsymbol{\omega}^* = \boldsymbol{\omega}_{\mathrm{gyr}} + k_{\mathrm{b}}(\mathbf{b} \times \mathbf{b}^*) + k_{\mathrm{g}}(\mathbf{g} \times \mathbf{g}^*), \end{cases} \tag{33}$$

where $\boldsymbol{\psi}(R, \boldsymbol{\omega}, \mathbf{q})$ represents the term $J^{-1}(\boldsymbol{\tau}_{\mathrm{FB}}(R^*, \boldsymbol{\omega}^*) - \boldsymbol{\tau}_{\mathrm{FB}}(R, \boldsymbol{\omega}))$. This is possible because $\boldsymbol{\omega}^*$ is a (linear) function of R, $\boldsymbol{\omega}$ and R^*; R^* can in turn be written as $RR^{\mathrm{T}}R^* = RE$ and E is parameterized by $q \triangleq \phi_E$.

Since $\boldsymbol{\phi}(R, \boldsymbol{\omega}, \mathbf{q})$ is linear in $\boldsymbol{\omega}$ and $SO(3)$ is a compact Lie group, then Assumption 3 of Lemma 3 in Appendix B is also automatically satisfied (see Ref. [35], Assumption 3 for details). Recalling that also Assumptions 1 and 2 in Lemma 3 were satisfied (respectively, in (28) and (32)), then Lemma 3 guarantees that the system (29) almost globally stabilizes the attitude at $(\bar{R}, 0) \in SO(3) \times so(3)$ and that convergence is asymptotic.

Remark 1 (π-rotations). The chosen Lyapunov function (31) proves convergence almost for all possible initial estimation errors $E(0)$. A question arises: what can be said about the initial configurations that are left out? Note first that, as clear from the definition of the logarithmic map, any configuration can be reached *via* a rotation about some axis by an angle less than or equal to π. The only configurations left out by the chosen Lyapunov function are those such that $\mathrm{trace}(E) \neq -1$, i.e., such that $\|\phi_E\| = \pi$. Such configurations correspond to the set of rotations about an arbitrary axis by an angle exactly equal to π and will be referred to as π-rotations.

The presence of unstable equilibria is inherently related to π-rotations. As a simple example, for the needle of a magnetic compass, the north direction is a stable equilibrium while the south direction (a π-rotation from the north) is an unstable one. In practice, due to the presence of noise, unstable equilibria are not an issue.

5.3. Simulation Results

The housefly body is modeled as an ellipsoid with mass $m = 10$ mg and moment of inertia $J = \mathrm{diag}\{J_x, J_y, J_z\}$, where $J_x = 0.13 \times 10^{-7}$ kg m^2, $J_y = 0.16 \times 10^{-7}$ kg m^2 and $J_z = 0.226 \times 10^{-7}$ kg m^2. Three independent sensors are considered for the attitude estimation: a three-axis gravitomer that measures the gravity vector (normalized without loss of generality to $g_0 = [0 \;\; 0 \;\; 1]^{\mathrm{T}}$ with respect to a right-handed space frame) components with respect to the body frame, a three-axis

magnetometer that measures the geomagnetic field vector (normalized without loss of generality to $b_0 = [1\ \ 0\ \ 0]^{\mathrm{T}}$) and a three-axis gyroscope that measures the angular velocity vector. Readouts from the gravitometer, magnetometer and gyroscope are simulated as follows:

$$\begin{aligned} \boldsymbol{\omega}_{\mathrm{gyro}} &= \boldsymbol{\omega}(t) + \mathbf{w}_1(t) \\ \mathbf{g}_{\mathrm{meas}}(t) &= P(s)R^{\mathrm{T}}(t)\mathbf{b}_0 + \mathbf{w}_2(t) \\ \mathbf{b}_{\mathrm{meas}}(t) &= R^{\mathrm{T}}(t-\tau_{\mathrm{d}})\mathbf{g}_0 + \mathbf{w}_3(t), \end{aligned} \tag{34}$$

where $\boldsymbol{\omega}(t)$ and $R(t)$ obey (29), and $\mathbf{w}_i(t) \in \mathbb{R}^3$ are zero-mean independent additive Gaussian noises with variance $\sigma_1^2 = 0.6$ and $\sigma_2^2 = \sigma_3^2 = 0.2$. With a little abuse of notation we indicate with $\mathbf{z}(t) = P(s)\mathbf{y}(t)$ the filtered version of the signal $\mathbf{y}(t)$, where $P(s)$ is the transfer function of a second-order low-pass filter which models the dynamics of the accelerometers inside the gravitometer. The variable τ_{d} (set to 30 ms in the simulation) represents a delay in the magnetic sensor outputs that models possible HW/SW measurement signal processing time. In the simulations we used $P(s) = \frac{\omega_n^2}{s^2+2\xi\omega_n s+\omega_n^2}$, where $\omega_n = 30$ and $\xi = 0.5$. The control torque $\boldsymbol{\tau}_{\mathrm{FB}}(R^*, \boldsymbol{\omega}^*)$ used in (33) was designed based on (20), where $k_\omega = 8$ and $K = 30I \in \mathbb{R}^{3\times 3}$.

Some closed-loop simulations results are shown in Fig. 9. During the simulation the body, starting from an orientation $R(0) \neq I$, i.e., $\phi_0 = \theta_0 = \psi_0 = \pi/4$, is driven

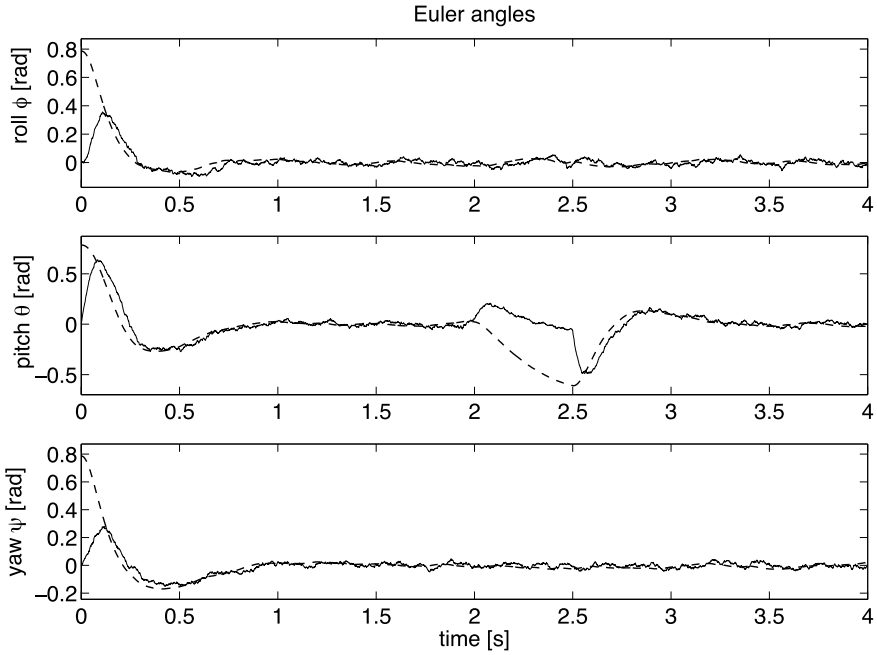

Figure 9. Actual Euler angles (dashed line) compared with their estimation (solid line) in a 4-s simulation.

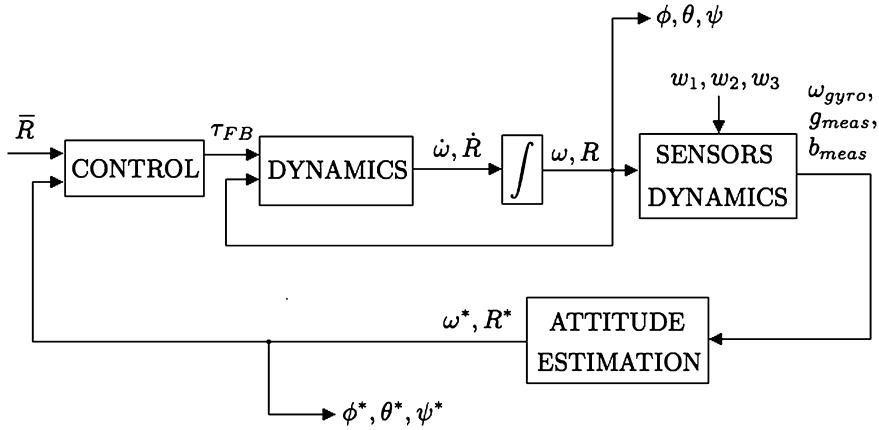

Figure 10. Schematic design of the control algorithm implementation.

by the control torque to the desired position $\overline{R}(t) = I$. A block diagram illustrating the control algorithm is presented in Fig. 10. For the sake of simplicity the continuous time version is presented here; in fact, a discretization of this algorithm is operated, using the Rodrigues formula (9) to guarantee $R(t)$ and $R^*(t)$ not to drif from $SO(3)$.

Since $R^*(0)$ is chosen to be the identity matrix I, the estimation initially differ from the actual position; thus, a transient in the attitude estimation is observed. Also, to simulate a linear acceleration of the body due for example to a transition from hovering to cruise, a 0.5 g disturbance lasting 0.5 s is introduced along the x-axis at time $t_1 = 2$ s (see Fig. 11). As a result, the estimated orientation is miscalculated, i.e., the acceleration is interpreted as a pitch-down rotation, therefore the controller produces a wrong pitch-up control input that creates a temporary displacement from the equilibrium position. Nonetheless, as soon as the disturbance disappears, the observer promptly settles on the correct value and the disturbance is effectively compensated for by the control algorithm.

6. Conclusions

In this work we presented a geometric (i.e., intrinsic and coordinate-free) approach to robust attitude estimation, derived from multiple and possibly redundant bioinspired navigation sensors, for attitude stabilization of a micromechanical flying insect.

Such a multimodal sensor fusion was implemented by a dynamic observer, in particular a complementary filter is proposed that is specialized to the nonlinear structure of the Lie group of rigid-body rotations.

The numerical implementation was also provided in the specific case of interest for inertial/magnetic navigation, i.e., when gravitometers, magnetometers and gyroscopes are available.

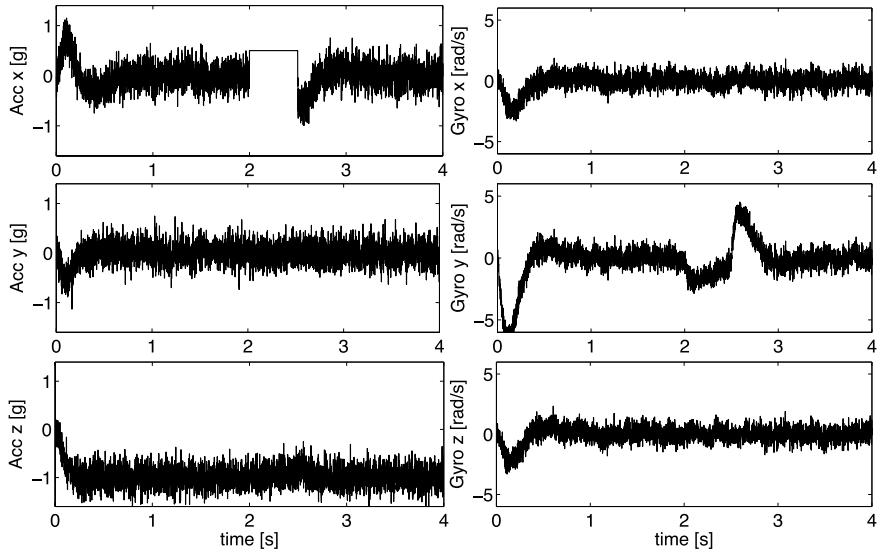

Figure 11. Data measured from the simulated accelerometers (left) and gyroscopes (right): a $0.5g$ disturbance is introduced in the accelerometer-x from $t_1 = 2$ s to $t_2 = 2.5$ s.

The performance of the proposed filter was experimentally tested. In particular, a 2-d.o.f. support was used to generate a known trajectory and compare it with the estimated trajectory from the filter, showing good performance.

We then merged the proposed filter with state-feedback attitude control techniques that were proven to provide a globally stable control system for body attitude based on a generalized separation principle valid for Lie groups. Moreover, the proposed controller does not depend on the specific choice of coordinates, thus leading to easy and robust implementation on robotic flying insects.

As future work, theoretical performance properties of the proposed observer will be analyzed in the presence of noisy data and disturbances (e.g., non-inertial accelerations, geomagnetic field distortion, etc.). The filter will be also tested in more realistic conditions: miniaturized inertial/magnetic systems will be mounted onboard of small flying vehicles as well as biomimetic swimming robots.

References

1. R. S. Fearing, K. H. Chiang, M. H. Dickinson, D. L. Pick, M. Sitti and J. Yan, Wing transmission for a micromechanical flying insect, in: *Proc. IEEE Int. Conf. on Robotics and Automation*, San Francisco, CA, Vol. 2, pp. 1509–1516 (2000).
2. M. H. Dickinson, F. O. Lehnmann and S. S. Sane, Wing rotation and the aerodynamic basis of insect flight, *Science* **284**, 1954–1960 (1999).
3. R. J. Wood, Design, fabrication and analysis, of a 3DOF, 3 cm flapping-wing MAV, in: *Proc. IEEE/RSJ Int. Conf. on Intelligent Robotics and Systems*, San Diego, CA, pp. 1576–1581 (2007).
4. R. J. Wood, The first takeoff of a biologically-inspired at-scale robotic insect, *IEEE Trans. Robotics* **24**, 341–347 (2008).

5. G. K. Taylor, Mechanics and aerodynamics of insect flight control, *Biol. Rev.* **76**, 449–471 (2001).
6. X. Deng, L. Schenato, W. C. Wu and S. S. Sastry, Flapping flight for biomimetic robotic insects. Part I: system modeling, *IEEE Trans. Robotics* **22**, pp. 789–803 (2006).
7. X. Deng, L. Schenato and S. S. Sastry, Flapping flight for biomimetic robotic insects. Part II: flight control design, *IEEE Trans. Robotics* **22**, 789–803 (2006).
8. P. Vela, K. Morgansen and J. W. Burdick, Trajectory stabilization for a planar carangiform fish, in: *Proc. IEEE Int. Conf. on Robotics and Automation*, Washington, DC, Vol. 1, pp. 756–762 (2002).
9. L. Schenato, W. C. Wu and S. S. Sastry, Attitude control for a micromechanical flying insect *via* sensor output feedback, *IEEE Trans. Robotics Automat.* **20**, 93–106 (2004).
10. H. Rifai, N. Marchand and G. Poulin, Bounded attitude control of a biomimetic flapping robot, in: *Proc. IEEE Int. Conf. on Robotics and Biomimetics*, Sanya, pp. 1–6 (2007).
11. M. Epstein, S. Waydo, S. B. Fuller, W. Dickson, A. Straw, M. H. Dickinson and R. M. Murray, Biologically inspired feedback design for *Drosophila* flight, in: *Proc. IEEE Am. Control Conf.*, New York, NY, pp. 3395–3401 (2007).
12. V. I. Arnold, *Mathematical Methods of Classical Mechanics*, 2nd edn. Springer, New York, NY (1989).
13. R. M. Murray, Z. Li and S. S. Sastry, *A Mathematical Introduction to Robotic Manipulation*. CRC Press, Boca Raton, FL (1994).
14. T. Frankel, *The Geometry of Physics: An Introduction*. Cambridge University Press, Cambridge (1997).
15. S. S. Sastry, *Nonlinear Systems: Analysis, Stability and Control*. Springer, New York, NY (1999).
16. F. Bullo and A. D. Lewis, *Geometric Control of Mechanical Systems*. Springer, New York, NY (2005).
17. F. Bullo and R. F. Murray, Proportional derivative (PD) Control on the Euclidean Group, *Technical Report*. California Institute of Technology, Anaheim, CA (1995).
18. S. P. Sane, The aerodynamics of insect flight, *J. Exp. Biol.* **206**, 4191–4208 (2003).
19. J. Chahl, Bioinspired engineering of exploration systems: a horizon sensor/attitude reference system based on the dragonfly ocelli for mars exploration applications, *J. Robotic Syst.* **20**, 35–42 (2003).
20. R. Hengstenberg, Mechanosensory control of compensatory head roll during flight in the blowfly *Calliphora erythrocephala*, *J. Comp. Physiol. A* **163**, 151–165 (1988).
21. G. Nalbach, The halteres of the blowfly *Calliphora*: I. Kinematics and dynamics, *J. Comp. Physiol. A* **173**, 293–300 (1993).
22. W. C. Wu, R. J. Wood and R. F. Fearing, Halteres for the micromechanical flying insect, in: *Proc. IEEE Int. Conf. on Robotics and Automation*, Washington, DC, Vol. 1, pp. 60–65 (2002).
23. Absoluteastronomy.com, http://www.absoluteastronomy.com/topics/Halteres.
24. M. H. Dickinson, Linear and nonlinear encoding properties of an identified mechanoreceptor on the fly wing measured with mechanical noise stimuli, *J. Exp. Biol.* **151**, 219–244 (1990).
25. H. Schuppe and R. Hengstenberg, Optical properties of the ocelli of *Calliphora erythrocephala* and their role in the dorsal light response, *J. Comp. Biol. A* **173**, 143–149 (1993).
26. B. Krylov, Ekaweeka.com, https://www.ekaweeka.com/1251/gallery/9028/?show=post_comment.
27. W. Reichardt and M. Egelhaaf, Properties of individual movement detectors as derived from behavioural experiments on the visual system of the fly, *Biol. Cybernet.* **58**, 287–294 (1988).
28. D. Lambrinos, H. Kobayashi, R. Pfeifer, M. Maris, T. Labhart and R. Wehner, Adaptive behavior of an autonomous agent navigating with a polarized light compass, *Adapt. Behav.* **6**, 131–161 (1997).

29. E. Wajnberga, G. Cernicchiaroa, D. Acosta-Avalosb, L. J. El-Jaicka and D. M. S. Esquivel, Induced remanent magnetization of social insects, *J. Magnet. Magnet. Mater.* **226–230**, 2040–2041 (2001).
30. W. C. Wu, L. Schenato, R. J. Wood and R. F. Fearing, Biomimetic sensor suite for flight control of MFI: design and experimental results, in: *Proc. IEEE Int. Conf. on Robotics and Automation*, Taipei, Vol. 1, pp. 1146–1151 (2003).
31. R. G. Brown and P. Y. C. Hwang, *Introduction to Random Signals and Applied Kalman Filtering*. Wiley, New York, NY (1992).
32. F. Daum, Nonlinear filters: beyond the Kalman filter, *IEEE A&E Syst. Mag.* **20** (8), 57–69 (2005).
33. D. Campolo, L. Schenato, L. Pin, X. Deng and E. Guglielmelli, Attitude stabilization of biologically inspired micromechanical flying insects. Part I: attitude estimation *via* multimodal sensor fusion, *Adv. Robotics (Special Issue on Biomimetic Robotics)* **23**, 955–977 (2009).
34. D. H. S. Maithripala, J. M. Berg and W. P. Dayawansa, An intrinsic observer for a class of simple mechanical systems on a lie group, *SIAM J. Control Optim.* **44**, 1691–1711 (2005).
35. D. H. S. Maithripala, J. M. Berg and W. P. Dayawansa, Almost-global tracking of simple mechanical systems on a general class of lie groups, *IEEE Trans. Automatic Control* **51**, 216–225 (2006).
36. D. E. Koditschek, The application of total energy as a Lyapunov function for mechanical control systems, *Dyn. Control Multibody Syst.* **97**, 131–157 (1989).
37. F. Bullo and R. M. Murray, Tracking for fully actuated mechanical systems: a geometric framework, *Automatica* **35**, 17–34 (1999).

Appendix

Appendix A. Complementary Filtering on $SO(3)$

Consider $N \geqslant 2$ homogenous and time-invariant vector fields $\vec{v}_1, \vec{v}_2, \ldots, \vec{v}_N$ (e.g., the gravitational field, the geomagnetic field, the light direction, etc.) and assume that at least two of them (e.g., $\vec{v}_1$ and $\vec{v}_2$, without loss of generality) are independent, which can be expressed in any coordinate frame as:

$$\vec{v}_1 \times \vec{v}_2 \neq 0. \tag{A.1}$$

Definition 1. *Given a rigid body, define a body frame $\mathcal{B}$ on it. Let the rigid body be at rest at some time t_0 and define thus a space frame $\mathcal{S}_0$ as the one coincident with the body frame $\mathcal{B}$ at time t_0. Let the constant vectors $\mathbf{v}_{i0} = [v_{i0x} \;\; v_{i0y} \;\; v_{i0z}]^{\mathrm{T}}$ represent the components of each vector field at time t_0 as measured by a set of sensors on the rigid body. At any time t, let $R(t) : \mathbb{R} \to SO(3)$ be a twice-differentiable function representing the orientation of the rigid body in 3-D space with respect to the space frame $\mathcal{S}_0$, let $\mathbf{v}_i = [v_{ix} \;\; v_{iy} \;\; v_{iz}]^{\mathrm{T}}$ be the (time-variant) components of each field and let $\boldsymbol{\omega}_{\mathrm{gyr}}$ be readouts of the gyroscopes; both $\mathbf{v}_i$ and $\boldsymbol{\omega}_{\mathrm{gyr}}$ are referred to the (body) moving frame.*

Lemma 1. *The trajectory $R(t) \in SO(3)$, defined as in Definition* 1*, is reflected in the measurements of the gyroscopes and of the vector fields sensors and can be*

expressed as:

$$\begin{cases} \widehat{\boldsymbol{\omega}}_{\text{gyr}} = R^{\text{T}}\dot{R} = \widehat{\boldsymbol{\omega}} \\ \mathbf{v}_i = R^{\text{T}}\mathbf{v}_{0i}. \end{cases} \tag{A.2}$$

Lemma 2. *Let $R(t):\mathbb{R} \to SO(3)$ represent, as in Definition* 1*, the trajectory on $SO(3)$ of a rigid body embedding a set of gyroscopes and let the angular velocity $\boldsymbol{\omega}$ of the rigid body be available, as in* (A.2)*, via readings from such gyroscopes. Let $R^{*\text{T}}\dot{R}^* = \widehat{\boldsymbol{\omega}}$ denote the dynamics of an estimator, then the tracking error:*

$$E \triangleq R^{\text{T}}R^*, \tag{A.3}$$

is such that $\|E(t)\|_{SO(3)} = \text{constant}$. In particular, the following identity holds:

$$\langle\langle \log(E), -E^{\text{T}}\widehat{\boldsymbol{\omega}}E + \widehat{\boldsymbol{\omega}}\rangle\rangle_{so(3)} = 0. \tag{A.4}$$

Theorem 1. *Let $R(t):\mathbb{R} \to SO(3)$ represent the orientation of the rigid body as in Definition* 1*. Let $R^*(t)$ denote the estimate of $R(t)$ and let it be defined by the following observer:*

$$\begin{cases} \dot{R}^* = R^*\widehat{\boldsymbol{\omega}}^* \\ \boldsymbol{\omega}^* = \boldsymbol{\omega}_{\text{gyr}} + \sum_{i=1}^{N} k_i(\mathbf{v}_i \times \mathbf{v}_i^*) \\ \mathbf{v}_i^* = R^{*\text{T}}\mathbf{v}_{0i}, \end{cases} \tag{A.5}$$

where $k_i > 0$ are the filter gains, and $\boldsymbol{\omega}_{\text{gyr}}$ and $\mathbf{v}_i$ represent the sensor readings as in (A.2)*.*

The observer (A.5) *asymptotically tracks $R(t)$ for almost any initial condition $R^*(0) \neq R(0)$ and in particular:*

$$\lim_{t\to\infty} R^{\text{T}}(t)R^*(t) = I. \tag{A.6}$$

Appendix B. Separation Principle on $SO(3)$

Here, the Lemma presented in Ref. [34] (Corollary 2) and proved in Ref. [35] for a general Lie group G is restated for the specific case of interest $G = SO(3)$.

Consider the system:

$$\begin{cases} \dot{R} = R\boldsymbol{\omega} \\ \dot{\boldsymbol{\omega}} = J^{-1}(J\boldsymbol{\omega} \times \boldsymbol{\omega} + \boldsymbol{\tau}_{\text{FB}}(R, \boldsymbol{\omega})) + \boldsymbol{\psi}(R, \boldsymbol{\omega}, \mathbf{q}), \end{cases} \tag{B.1}$$

with $(R, \widehat{\boldsymbol{\omega}}) \in SO(3) \times so(3)$ and $\mathbf{q} \in \mathbb{R}^n$ and $V = U(R) + \frac{1}{2}\langle\langle \widehat{\boldsymbol{\omega}}, \widehat{\boldsymbol{\omega}}\rangle\rangle_{so(3)}$, where $U(R)$ is a smooth globally defined Morse function representing the potential energy of the system. Also consider the following assumptions.

Assumption 1. *The point $(\bar{R}, 0)$ is an almost globally stable equilibrium point of* (B.1) *with $\boldsymbol{\psi} \equiv 0$ and furthermore:*

$$\langle\langle R^{\text{T}} \operatorname{grad} U, \widehat{\boldsymbol{\omega}}\rangle\rangle_{so(3)} + \langle\langle J^{-1}\widehat{\boldsymbol{\tau}}_{\text{FB}}, \widehat{\boldsymbol{\omega}}\rangle\rangle_{so(3)} \leqslant 0. \tag{B.2}$$

Condition (B.2) is satisfied by any simple mechanical system with potential energy $U(R)$ and Rayleigh-type dissipation. The equilibrium $(\bar{R}, 0)$ is an almost globally stable equilibrium if $\bar{R}$ is a unique minimum of $U(R)$.

Assumption 2. *The function* $\mathbf{q}(t) \in \mathbb{R}^n$ *satisfies:*

$$\|\mathbf{q}(t)\| \leqslant c\|\mathbf{q}(0)\|e^{-\lambda t}, \tag{B.3}$$

for some $c > 0$, $\lambda > 0$ *and all* $t > 0$.

Assumption 3. *The interconnection term satisfies* $\boldsymbol{\psi}(R, \boldsymbol{\omega}, 0) \equiv 0$ *and the linear growth conditions:*

$$\|\boldsymbol{\psi}\| \leqslant \gamma_1(\|\mathbf{q}\|)\|\boldsymbol{\omega}\| + \gamma_2(\|\mathbf{q}\|), \tag{B.4}$$

for two $\mathcal{K}_\infty$ *functions* $\gamma_1(\cdot)$ *and* $\gamma_2(\cdot)$.

Lemma 3. *If the Lie group G is compact and if Assumptions* 1–3 *are satisfied, then the equilibrium* $(\bar{R}, 0)$ *of the system* (B.1) *is almost-globally stable. Convergence is asymptotic if the inequality in Assumption* 1 *is strict.*

About the Authors

Domenico Campolo is currently Assistant Professor at Nanyang Technological University in Singapore. He received his Laurea Degree from the University of Pisa, in 1998, and the Diploma Degree from Scuola Superiore Sant'Anna, in 1999. In 2002, he earned his PhD (Diploma di Perfezionamento) in Micro-Engineering from Scuola Superiore Sant'Anna, Pisa, while working at MiTech Lab (currently the CRIM Lab). During Fall 1998, he was working at the EECS Deptartment of ZheJiang University, HangZhou, P. R. China as a visiting graduate student. In the period 2000–2003, he was at UC Berkeley (USA) as a Visiting Scholar and, after 2002, as a Post-doc working on the MFI (Micromechanical Flying Insect) project. During 2003–2009, he worked as a Post-doc at Campus Bio-Medico University in Rome (Italy), Bioengineering Department, involved in both teaching and research. His research interests include mechatronic technologies with application to the new emerging fields of phenomics and neuro-developmental engineering, in both animal and human models; biomimetic microrobotics, including: design, fabrication, development and control of biologically inspired smart actuators and sensors; micro/nano-manipulation; and micro/nano-fabrication.

Giovanni Barbera received the BS degree in Automation Engineering from the University of Padova, in 2006. Currently, he is attending the MS degree at the University of Padova. His research interests are in bioinspired vehicle design and control, autonomous navigation, trajectory tracking algorithms, and coordination and cooperation in multi-agent systems.

Luca Schenato received the DE degree in Electrical Engineering from the University of Padova in 1999, and the PhD degree in Electrical Engineering and Computer Sciences from UC Berkeley, in 2003. From January 2004 to August, he was a Post-doctoral scholar at UC Berkeley. Currently he is Associate Professor at the Information Engineering Department at the University of Padova. His interests include swarm robotics and biomimetic locomotion, networked control systems, wireless sensor networks, and distributed control. He was awarded the 2004 Researchers Mobility Fellowship by the Italian Ministry of Education, University and Research (MIUR), and the 2006 Eli Jury Award in UC Berkeley.

Lijuan Pi received her BS degree from the Department of Automation of Tianjin Univeristy, China. She received her MS degree in Mechanical Engineering of the University of Delaware, in 2009. Her research centered on bioinspired robotic fish development.

Xinyan Deng received her BS degree from the Department of Automation of Tianjin University, P. R. China. She received her PhD degree from the Mechanical Engineering Department of UC Berkeley, in 2004. Since then she has been an Assistant Professor at the Department of Mechanical Engineering at the University of Delaware. Her research interest is in the principles of aerial and aquatic locomotion in animals and robots, including experiment fluid mechanics, dynamics and control, and bioinspired systems. She received an NSF CAREER Award in 2006.

Eugenio Guglielmelli received the Laurea degree (Master) in Electronics Engineering and the PhD in Elctronics, Telecommunications and Computer Science (Biomedical Robotics track) from the University of Pisa (Italy), in 1991 and 1995. He is currently Associate Professor of Bioengineering at Università Campus Bio-Medico (Roma, Italy) where he serves as the Head of the Laboratory of Biomedical Robotics and Biomicrosystems. From 1991 to 2004, he worked with Professor Paolo Dario at the Advanced Robotics Technology & Systems Laboratory (ARTS Lab) of the Scuola Superiore Sant'Anna (Pisa, Italy), that he directed from 2002 to 2004. His main current research interests are in the fields of human-centred robotics, biomechatronic design and biomorphic control of robotic systems, and in their application to robot-mediated motor therapy, assistive robotics, and neurorobotics. He is author/co-author of more than 150 papers appeared on peer-reviewed international journals, conference proceedings and books. He currently serves as Associate Editor of the *IEEE Robotics and Automation Magazine* and on the Editorial Board of the *International Journal on Applied Bionics and Biomechanics*. He has been Guest Co-Editor of the Special Issues on Rehabilitation Robotics of the *IEEE Transactions on Robotics* and *Autonomous Robots*, and also of the Special Issue on Robotics Platforms for Neuroscience of *Advanced Robotics*. He is principal investigator/partner of several national and international projects in the area of biomedical robotics. He is member of the IEEE Robotics and Automation Society, of the IEEE Engineering in Medicine and Biology Society and of the Society for Neuroscience. He is currently Associate Vice-President for Technical Activities of the IEEE Robotics and Automation Society (RAS) and he also served as Co-chair of the Technical Committee on Rehabilitation and Assistive Robotics (2004–2007) and as RAS Secretary (2002–2003) of the same society. He was/is member of the Organizing Committees of HURO1998, ICAR2003, IROS2004, IFAC/SYROCO2006, ICRA2007 and ROMAN2009, and of the Programme Committees of several international conferences, workshops and symposia.